J. Mech. Phys. Solids 179 (2023) 105395

Contents lists available at ScienceDirect

Journal of the Mechanics and Physics of Solids

journal homepage: www.elsevier.com/locate/jmps

Nonequilibrium thermodynamic modeling of case II diffusion in glassy polymers

Zhaoqiang Song [a,b,*], Xu Li [a,c], Kaijin Wu [d], Shengqiang Cai [a,*]

[a] Department of Mechanical and Aerospace Engineering, University of California, San Diego, La Jolla, CA 92093, United States
[b] Department of Material Science and Engineering, University of Pennsylvania, Philadelphia, PA 19104, United States
[c] School of Science, Hubei Key Laboratory of Theory and Application of Advanced Materials Mechanics, Wuhan University of Technology, Wuhan, 430070, China
[d] Department of Modern Mechanics, University of Science and Technology of China, Hefei, Anhui 230026, China

ARTICLE INFO

Keywords:
Case II diffusion
Glassy polymer
Thermodynamic modeling
Thin film
Core-shell structure

ABSTRACT

In this article, we formulate a nonequilibrium thermodynamic theory for case II diffusion in a glassy polymer. In the model, we integrate the three-dimensional elasto-visco-plasticity of a glassy polymer, the Flory-Rehner theory for polymer network swelling, and the kinetics law for solvent migration with the concentration-dependent diffusivity. Our theory is given in a general 3D tensorial form, which, therefore, can be used to model case II diffusion in glassy polymers with arbitrary geometries and under different mechano-chemical loading conditions. An intrinsic length determined by the combination of the polymer viscosity and solvent diffusivity arises from the theory, which dictates the size-dependent case II diffusion in glassy polymers. The theory developed in the article may provide important guidance for designing semi-permeable membranes, waterproof coating, and drug-delivery systems, where case II diffusion can commonly occur.

1. Introduction

Solvent diffusion in glassy polymers can be commonly seen in many practical applications, such as semipermeable membranes (Baker and Lokhandwala, 2008; Baker and Low, 2014), waterproof coating (Zhao et al., 2019; Zou et al., 2021) and drug delivery systems (Colombo et al., 2000), as shown in Fig. 1. Depending on the interaction between the solvent molecules and the polymer chains, the diffusion can be categorized as Fickian diffusion and non-Fickian diffusion (Ercken et al., 1996; Hajova et al., 2013). In contrast to Fickian diffusion, non-Fickian diffusion in glassy polymers often exhibits a sharp diffusion front, and the amount of solvent adsorbed by the glassy polymer increases linearly with time (Thomas and Windle, 1982). This type of diffusion is also often classified as case II diffusion, which usually occurs when the solvent behaves like a plasticizer for the glassy polymer (Nealey et al., 1995; Zhou et al., 2001).

In the past, a series of experiments have been conducted on case II diffusion in glassy polymers. The examples of case II diffusion systems include Polymethyl methacrylate (PMMA) with methanol (Ercken et al., 1996; Hui et al., 1987a, b; More et al., 1992; Nixdorf et al., 2019; Thomas and Windle, 1978), Polystyrene (PS) with alkane (Nealey et al., 1995; P. Gall et al., 1990; Zhou et al., 2001) and Polyvinyl chloride (PVC) with acetone (Perry et al., 1994). Experimental studies have revealed that the sharp diffusion front observed

* Corresponding authors.
E-mail addresses: zhs084@ucsd.edu (Z. Song), shqcai@ucsd.edu (S. Cai).

https://doi.org/10.1016/j.jmps.2023.105395
Received 15 June 2023; Received in revised form 22 July 2023; Accepted 22 July 2023
Available online 26 July 2023

Nomenclature

C	Concentration of solvent
D	Diffusion coefficient
D_0	Prefactor of D
$D_{jm}^{A,p}$	Rate of the plastic shape change of element "A"
De	Deborah number
$\mathbf{F}$, F_{iK}	Deformation gradient
F_{iK}^{A}	Deformation gradients of element "A"
$F_{iK}^{A,\,p}$	Plastic component of F_{iK}^{A}
$F_{iK}^{A,e}$	Elastic component of F_{iK}^{A}
F_{iK}^{B}	Deformation gradient of element "B"
H_{iK}	$= \frac{1}{\det(\mathbf{F})} \frac{\partial det(\mathbf{F})}{\partial F_{ik}}$
J	$= \det(\mathbf{F})$, volume change
$J^{A,p}$	$= \det(\mathbf{F}^{A,p})$
J^{A}	$= \det(\mathbf{F}^{A})$
$\dot{j}_p$	Plastic volume expansion rate
L_c	Critical length at which the characteristic diffusion time is comparable to the characteristic relaxation time of plastic flow
L_c^{max}	Maximum critical length of L_c
m	Material property
M	$= mn$, material property
M_s	Number of solvent molecules
n	Exponential factor
$N_{ij}^{A,p}$	Direction tensor of element "A"
p^A	Hydrostatic pressure of element "A"
s	Athermal shear strength of the gel
s_0	Athermal shear strength of the dry glassy polymer
s_{ij}^{A}	Deviatoric stress tensor of element "A"
s_{iK}	First Piola-Kirchhoff stress
W	Free energy density of the gel
W_{mix}	Free energy density due to the mixing of the polymer chains and the solvent
$W_{stretch}$	Free energy density due to the stretching of the network
$\dot{\gamma}$	Equivalent plastic shear strain rate for the primary relaxation process
$\dot{\gamma}_0$	Prefactor of $\dot{\gamma}$
ζ_α, ζ_β	Internal variables
η_0	Bulk viscosity of the dry glassy polymer
Θ	Characteristic diffusion time
Λ	Characteristic relaxation time
λ_{eq}	Stretch of fully swollen polymer in the equilibrium state
λ_{i0}^{p}	Initial plastic stretch along x_i
μ	Chemical potential of solvent in the polymer
μ_0	Chemical potential of unmixed pure solvent
μ_A	Shear modulus of element "A"
μ_B	Shear modulus of element "B"
μ_{dry}	Chemical potential of the dry polymer
σ_{ij}^{A}	Stress component of element "A"
σ_{ij}^{B}	Stress component of element "B"
σ_{ij}	Cauchy (true) stress
Π	Stress component due to the mixing of the polymer chains and the solvent
τ^A	Equivalent shear stress of element "A"
ϕ	Volumetric fraction of solvent
χ	Flory interaction parameter
Ω	Volume per solvent molecule
$(\cdot)$	Time derivative

in case II diffusion in a glassy polymer can be ascribed to the decrease of the glass-transition temperature of the polymer after swelling (Ercken et al., 1996). When a glassy polymer sphere is submerged into solvent, a core-shell structure can form, with a swollen rubbery outer shell and a dry glassy inner core (Foreman and Vollmer, 2015; Li and Lee, 2006). It has also been acknowledged that the interplay between the viscoelasticity of the polymer network and solvent migration dynamics within the polymer network determines the main features of case II diffusion (Argon et al., 1999; Thomas and Windle, 1982).

To understand the formation of the sharp diffusion front and other characteristics in case II diffusion, tremendous modeling efforts have been made. Thomas and Windle (1982) were among the first to model the formation of the sharp diffusion front during case II diffusion by assuming the viscosity of a glassy polymer decreases with the increase of the solvent concentration. Building upon their work, Hui et al. (1987a, b) obtained an asymptotic solution describing transient state and steady state of case II diffusion, with considering the effect of the osmosis. Hui et al. (1987b) also pointed out that the assumption of a linear rheological behavior of glassy polymers adopted in their model may be oversimplified. Thereafter, Argon et al. (1999) considered a more realistic rheological model for visco-plastic flow of glassy polymers and developed a mechanistic model that accounts for the coupled diffusion and elasto-visco-plastic deformation rates associated with the self-similar propagation front. However, most of the previous models were developed specifically for certain geometries (e.g., thin film, half space), and typically assumed that the polymers were either stress free or subjected to simple mechanical constraints. Though these models have successfully explained some features of case II diffusion in glassy polymers, additional efforts are required to formulate a more general model for case II diffusion in glassy polymers with arbitrary geometries and subjected to complex loading conditions. Moreover, recent experiments have shown that case II diffusion in a glassy polymer is size-dependent. For instance, at room temperature, the moving velocity of the diffusion front for the system of n-hexane in PS increases from 0.036 $\mu m/hr$ to 1.33 $\mu m/hr$ as the thickness of the polymer film decreases from 20 μm to 158 nm (Ogieglo et al., 2013; P. Gall et al., 1990). Similarly, faster moving velocity of the diffusion front of methanol have been observed in smaller PMMA beads (Li and Lee, 2006). However, the size-dependent effects observed in case II diffusion remains unexplained (Li and Lee, 2006).

In this article, we aim to formulate a general 3D model for case II diffusion in glassy polymers. We incorporate the nonequilibrium thermodynamics of solvent diffusion, the Flory-Rehner theory for polymer network swelling and the three-dimensional elasto-visco-plastic model of the glassy polymer. The theory is generally applicable for modeling case II diffusion of solvent in glassy polymers with arbitrary shapes and subjected to any loading conditions. Herein, we also compare our theoretical predictions with different experiments to demonstrate the validity of the model. The outline of this article is as follows. The governing differential equations for case II diffusion are presented in Section 2. Section 3 applies the model to study case II diffusion in a laterally constrained thin film. Section 4 applies the model to study case II diffusion in a polymer sphere. Section 5 discusses size effects in case II diffusion based on the simple scaling analysis. Finally, Section 6 provides a conclusion.

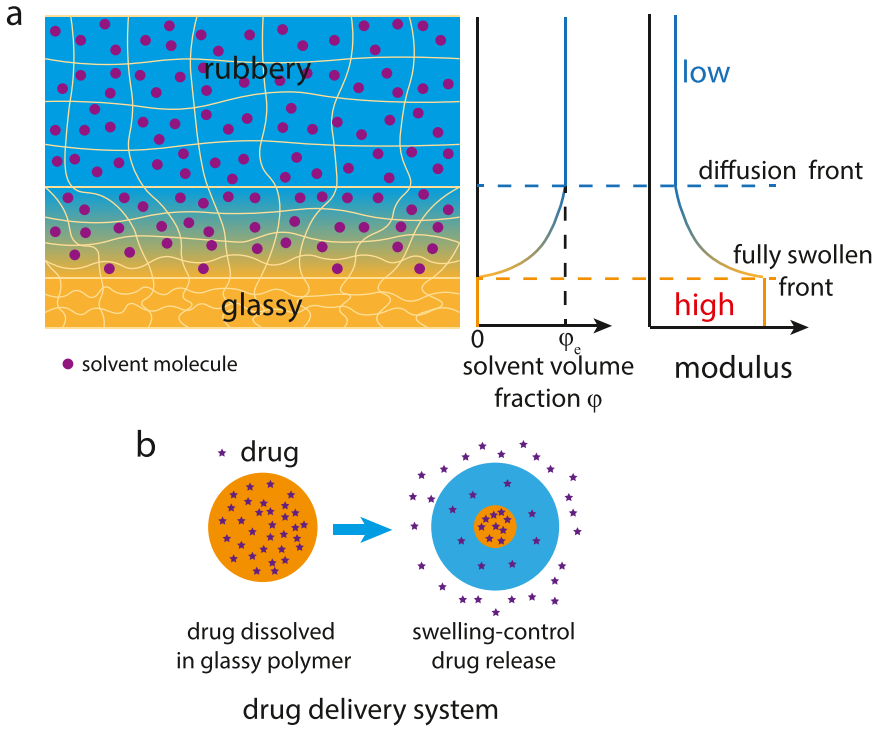

Fig. 1. (a) Schematic of case II diffusion in the glassy polymer. After swelling, the polymer becomes rubbery, and as a result, its modulus dramatically decreases. (b) The application of case II diffusion in drug delivery systems.

2. Theory

In this section, we develop a nonequilibrium thermodynamics model for non-Fickian diffusion of solvent in a glassy polymer which is also subjected to mechanical loadings. As shown in Fig. 2, a polymer (in the glassy state when it is dry), the external forces, and the solvent-containing environment together form a composite thermodynamic system. The system exchanges energy with the rest of the world by heat, but not by work; and it does not exchange matter with the rest of the world.

2.1. Constitutive model of a glassy polymer containing solvent

Fig. 2a illustrates a block of a dry glassy polymer with volume denoted by V. When the dry polymer is subjected to mechanical forces and in contact with a solvent, the polymer can deform and imbibe solvent (Fig. 2b). In an isothermal condition, the second law of thermodynamics requires that:

$$\delta W \le s_{iK}\delta F_{iK} + (\mu - \mu_0)\delta C, \tag{1}$$

where W is the free energy density of the gel (the polymer mixed with solvent molecules), which depends on the deformation gradient F_{iK}, the concentration of solvent C, and other internal variables as

$$W = W\left(F_{iK}, C, \zeta_\alpha, \zeta_\beta, \ldots\right) \tag{2}$$

and $C = \frac{M_s}{V}$ with M_s being the number of solvent molecules, μ_0 is the chemical potential of unmixed pure solvent, μ is the chemical potential of solvent in the polymer, F_{iK} is the deformation gradient, s_{iK} is the first Piola-Kirchhoff stress, and ζ_α and ζ_β are the internal variables describing the kinetic and dissipation processes inside the polymer. We will specify these internal variables later. Combining Eq. (1) and Eq. (2), we obtain the following inequality:

$$\frac{\partial W}{\partial F_{iK}}\delta F_{iK} + \frac{\partial W}{\partial C}\delta C + \sum_\alpha \frac{\partial W}{\partial \zeta_\alpha}\delta\zeta_\alpha - s_{iK}\delta F_{iK} - (\mu - \mu_0)\delta C \le 0. \tag{3}$$

We adopt molecular incompressibility assumption, so the change of volume between the current state and the reference state is the volume of the absorbed solvent, i.e.

$$\Omega C = \det(\mathbf{F}) - 1, \tag{4}$$

where Ω is the volume per solvent molecule.

Following the Coleman–Noll procedure in continuum mechanics, we require Eq. (3) to be satisfied independently for all conceivable physical processes (Gurtin et al., 2012), which results in the local mechanical equilibrium and chemical equilibrium (Hong et al., 2009):

$$s_{iK} = \frac{\partial W}{\partial F_{iK}} - \frac{\mu - \mu_0}{\Omega}\frac{\partial \det(\mathbf{F})}{\partial F_{iK}}, \tag{5}$$

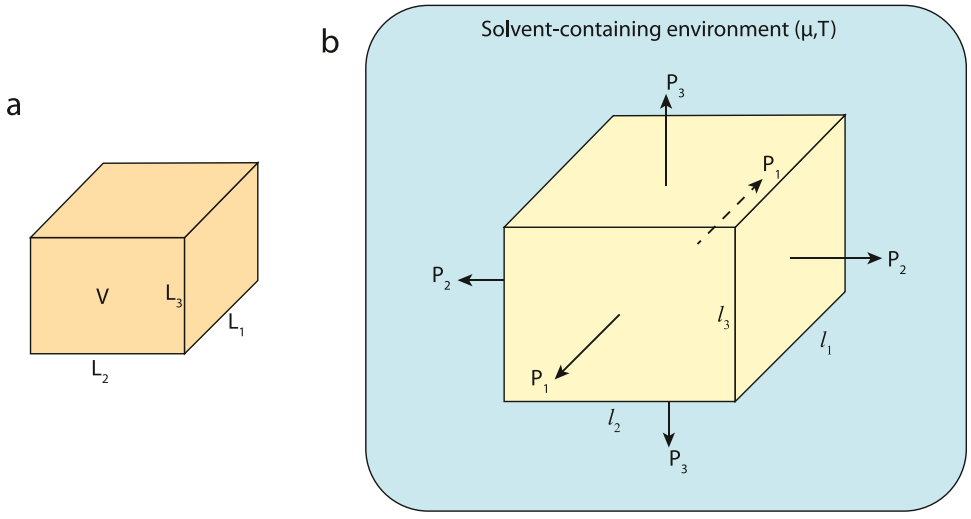

Fig. 2. (a) In the reference state, a dry polymer in the glassy state contains no solvent and is subject to no applied forces. (b) In the current state, the network is in equilibrium with applied forces, and with a solvent-containing environment of a fixed chemical potential of pure solvent and a fixed temperature.

and the nonequilibrium processes described by the internal variables:

$$\sum_{\alpha}\frac{\partial W}{\partial \zeta_{\alpha}}\dot{\zeta}_{\alpha} \le 0, \tag{6}$$

where $\dot{\zeta}_{\alpha}$ denotes the rate of internal variable ζ_{α}. In Eq. (5), we have $\frac{\partial det(\mathbf{F})}{\partial F_{ik}} = H_{iK}\det(\mathbf{F}) = \frac{1}{2}e_{ijk}e_{KLM}F_{jL}F_{kM}$.

The Cauchy (true) stress σ_{ij} is given as

$$\sigma_{ij} = \frac{s_{iK}F_{jK}}{\det(\mathbf{F})}. \tag{7}$$

Combined with Eq. (5), Eq. (7) is written as

$$\sigma_{ij} + \frac{\mu - \mu_0}{\Omega}\delta_{ij} = \frac{\partial W\left(F_{iK}, C, \zeta_{\alpha}, \zeta_{\beta}, \ldots\right)}{\partial F_{iK}}\frac{F_{jK}}{\det(\mathbf{F})}. \tag{8}$$

Following the Flory-Rehner theory (Flory and Rehner, 1943), we write the free energy of the polymer containing solvent as

$$W = W_{stretch} + W_{mix} \tag{9}$$

where W_{mix} is the free energy density due to the mixing of the polymer chains and the solvent and $W_{stretch}$ is the free energy density due to the stretching of the network.

The Helmholtz free energy of mixing is taken to be the form given by Flory (Flory, 1942)

$$W_{mix}(C) = -\frac{kT}{\Omega}\left[\Omega C\ln\left(1+\frac{1}{\Omega C}\right) + \frac{\chi}{1+\Omega C}\right], \tag{10}$$

where χ is the Flory interaction parameter.

The resistance to the deformation inside the polymer has two mechanisms: intermolecular resistance to chain-segment movement (elastic spring and viscoplastic dashpot, element "A" in Fig. 3), and entropic resistance to chain stretching (Langevin spring, element "B" in Fig. 3). To the first-order approximation, the proposed model only considers the relaxation process of element "A". As shown in Fig. 3, the parallel deformation gradients are the same:

$$F^{B}_{iK} = F^{A}_{iK} = F_{iK}. \tag{11}$$

We can further decompose the deformation gradient F^{A}_{iK} of element "A" into an elastic component $F^{A,e}_{iK}$ and a plastic component $F^{A,p}_{iK}$ (Lee, 1969),

$$F^{A}_{iK} = F^{A,e}_{iJ}F^{A,\,p}_{jK}. \tag{12}$$

The plastic volume change in element "A" is $J^{A,p} = \det(\mathbf{F}^{A,p})$. It is noted that for a glassy polymer only subjected to mechanical stresses, the volume change associated with its plastic deformation is usually assumed to be negligible (Mulliken and Boyce, 2006). Nevertheless, for case II diffusion, solvent diffusion can cause the significant volume change of the polymer.

The stretching of the network causes a reduction in the entropy of the network. The Helmholtz free energy due to the stretching of the network is taken to be (Flory, 1953)

$$W_{stretch} = \frac{1}{2}\mu_B[F_{iK}F_{iK} - 3 - 2ln(J)] + \frac{1}{2}\mu_A\left[\left(F^{A,e}_{iK}F^{A,e}_{iK}\right) - 3 - 2\ln\left(\frac{J^{A}}{J^{A,p}}\right)\right], \tag{13}$$

where μ_B is the shear modulus of element "B", μ_A is the shear modulus of element "A", and the elastic deformation of element "A" can be obtained from Eq. (12) as:

$$F^{A,e}_{iK} = F^{A}_{iJ}F^{A,p-1}_{jK}. \tag{14}$$

A combination of Eqs. (8–13) gives

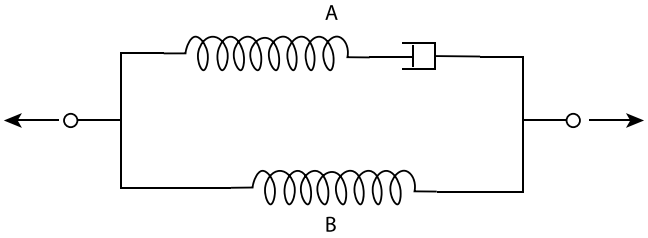

Fig. 3. Schematic of viscoelastic model (glassy polymer): element "**A**" represents glassy behavior, and element "**B**" represents rubbery behavior.

$$\sigma_{ij} + \frac{\mu - \mu_0}{\Omega}\delta_{ij} = \sigma_{ij}^{\mathrm{B}} + \sigma_{ij}^{A} + \Pi\delta_{ij}, \tag{15}$$

where the stress components are:

$$\sigma_{ij}^{\mathrm{B}} = \frac{\mu_B}{J}\left(F_{iK}F_{jK} - \delta_{ij}\right), \tag{16}$$

$$\sigma_{ij}^{A} = \frac{\mu_A}{J}\left(F_{iM}^{A}F_{mL}^{A,p-1}F_{lK}^{A,p-1}F_{jK} - \delta_{ij}\right), \tag{17}$$

and

$$\Pi = \frac{kT}{\Omega}\left[\ln\left(1 - \frac{1}{J}\right) + \frac{1}{J} + \frac{\chi}{J^2}\right], \tag{18}$$

in which $J = \det(\mathbf{F})$ is the volume change, and $H_{iK}F_{jK} = \delta_{ij}$.

2.2. Rate-dependent elasto-plasticity of a solvent-containing glassy polymer

The finite strain elasto-visco-plastic model of a solvent-containing glassy polymer adopted in the current study closely follows what presented by Bergstrom and Boyce (Bergstrom, 1998; Bergström and Boyce, 2000), and Boyce et al. (Boyce et al., 2001, 2000). It is noted that our elasto-visco-plastic model for glassy polymers only considers the primary relaxation process in the following derivation. The rate of plastic deformation of element "A" is given as

$$\dot{F}_{iK}^{A,p} = F_{iJ}^{A,e-1}D_{jm}^{A,p}F_{mL}^{A,e}F_{lK}^{A,p} \tag{19}$$

with the rate of the plastic shape change containing both the deviatoric and volumetric components:

$$D_{ij}^{A,p} = \dot{\gamma}N_{ij}^{A,p} + \dot{j}_p\delta_{ij}, \tag{20}$$

where

$$\dot{\gamma} = f\left(\tau^A, p^A\right) \tag{21}$$

is an equivalent plastic shear strain rate for the relaxation process,

$$\dot{j}_p = g\left(p^A\right) \tag{22}$$

is the plastic volume expansion rate, and

$$N_{ij}^{A,p} = s_{ij}^{A}\Big/\tau^A \tag{23}$$

is the direction tensor which is taken to be coaxial with the deviatoric stresses acting on intermolecular network (element "A"). In Eqs. (21–23),

$$p^A = \frac{1}{3}\sigma_{kk}^{A} \tag{24}$$

is the hydrostatic pressure, and

$$\tau^A = \sqrt{\frac{1}{2}s_{ij}^{A}s_{ij}^{A}} \tag{25}$$

is the equivalent shear stress, where

$$s_{ij}^{A} = \sigma_{ij}^{A} - p^A \tag{26}$$

is the deviatoric stress tensor.

We consider the deviatoric plastic strain rate of the glassy polymer to be given by a power-law (Argon et al., 1999; Loeffel and Anand, 2011)

$$\dot{\gamma} = \dot{\gamma}_0\left(\frac{\tau^A}{s}\right)^n, \tag{27}$$

where $\dot{\gamma}_0 = \dot{\gamma}_0^0\exp\left(-\frac{\Delta G}{kT}\right)$ with $\dot{\gamma}_0^0$ being the pre-exponential factor, ΔG being the activation energy and T being the temperature, n is the exponential factor, and s is the athermal shear strength.

For case II diffusion, the solvent often behaves like a plasticizer (Nealey et al., 1995; Zhou et al., 2001) for the glassy polymer. Therefore, the athermal plastic resistance (s) can be significantly lowered by the absorbed diluent as it reduces the intermolecular interactions. Often this reduction is taken to be of exponential form as (Argon et al., 1999; Thomas and Windle, 1982)

$$s = s_0 \exp(-m\phi), \tag{28}$$

where $\phi = \frac{\Omega C}{1+\Omega C}$ is the volumetric fraction of the solvent and s_0 is the athermal shear strength of the dry glassy polymer. Thus, the deviatoric plastic strain rate in the swollen polymer is written as

$$\dot{\gamma} = \dot{\gamma}_0 \left(\frac{\tau^A}{s_0}\right)^n \exp(M\phi), \tag{29}$$

where $M = mn$. Similarly, the equivalent plastic volumetric strain rate can be given as

$$\dot{j}_p = \frac{p^A}{\eta_0} \exp(M\phi), \tag{30}$$

where η_0 is the bulk viscosity of the dry glassy polymer, which describes the viscous resistance to the rate of volume change.

2.3. Solvent diffusion in the polymer

When the solvent diffuses in a glassy polymer, we adopt a linear kinetics law between the volumetric flux of solvent ($\vec{j}\Omega$) and the chemical potential gradient as

$$\vec{j} = -\frac{CD}{kT}\vec{\nabla}\mu, \tag{31}$$

where D is the diffusion coefficient. It is reasonable to assume the diffusion coefficient to be dependent on volume fraction of solvent in the polymer: the higher volume fraction of solvent, the larger of the diffusion coefficient is. We simply adopt the Kozeny-Carman equation (Chapuis and Aubertin, 2003) for describing the diffusivity of porous media to assume that

$$D = D_0\phi^2, \tag{32}$$

where D_0 is the prefactor.

2.4. Material parameters

In the past, polystyrene (PS) with n-hexane and polymethyl methacrylate (PMMA) with methanol were the two systems which have been most intensively studied in the context of case II diffusion. The parameters of PS-hexane system and PMMA-methanol system used for the modeling are summarized in Table 1. It is noted that each material parameter listed in Table 1 is usually obtained from a single study, and the measurements of those parameters are based on specific models and assumptions adopted in those studies. To improve

Table 1
Parameters in the calculation of case II diffusion in the PS-hexane system (thin film) and the PMMA-methanol system (core-shell structure).

Parameter	notation	Values	Notes
Glassy modulus	μ_A	1 GPa	This number is taken from the reference (Argon et al., 1999). In the reference, it is the glassy modulus for PS. We use the same number for PMMA in this paper.
Rubbery modulus	μ_B	1 MPa	This number is estimated based on experimental data of PMMA from the reference (Mulliken and Boyce, 2006). This number is also used for PS in the current study.
Athermal shear strength	s_0	238 MPa	This number is taken from the reference (Argon et al., 1999). In the reference, it is the athermal shear strength for PS. We use the same number for PMMA in this paper.
Flory's interaction parameter	χ	1.3	This number comes from the PS-pentane system in the reference (Hajova et al., 2013). We use the same number for PS-hexane and PMMA-methanol systems.
Exponential factor	n	9	In the reference (Argon et al., 1999), the value of n is in a range between 7.3 and 8.8 for PS. In our current study, we use the same number for PS and PMMA as $n = 9$.
Material property	M	100 (PS) 90 (PMMA)	$M = mn$. For PS, the material constant m is in a range between 10 and 20 (Thomas and Windle,1981). Therefore, M in a range between 90 and 180 for PS. We use $M = 100$ for PS-hexane system and $M = 90$ for PMMA-methanol system in this paper.
Bulk viscosity	η_0	$10^{14} Pa \cdot s$	This number is taken from the reference (Chang et al., 2021). In the reference, it is the bulk viscosity for PS. We use the same number for PMMA system in this paper.
Prefactor	$\dot{\gamma}_0$	$10^{12}\ s^{-1}$	This prefactor is estimated based on the strain rate pre-factor of PS in the reference (Argon et al., 1999). This number is also used for PMMA system in current study.
Prefactor of diffusion coefficient	D_0	$3 \times 10^{-15}\ m^2/s$ (PS) $3 \times 10^{-11}\ m^2/s$ (PMMA)	The pre-factor of diffusion coefficient is estimated based on the reference (Argon et al., 1999; Ercken et al., 1996). More details are given in Section 2.4.

the agreement between theoretical predictions from the current study and experimental measurements, we have made slight adjustments for some parameters. The polymer in the dry state has extremely low solvent concentration, and we assume that the chemical potential of solvent in the initially dry polymer is $\mu_{dry} - \mu_0 = -5.23 \times 10^{-20} J$.

The prefactors of the diffusion coefficients of PS-hexane and PMMA-methanol systems at room temperature are obtained based on the following estimation. The diffusion coefficient of $C_6H_{13}I$ in PS at $\phi = 0.14$ is known to be $1 \times 10^{-17} m^2/s$ (Argon et al., 1999), which implies a prefactor value of $D_0 = 5.2 \times 10^{-16} m^2/s$ according to Eq. (32). To account for the lower molecular weight of hexane (C_6H_{14}) compared to $C_6H_{13}I$, we use a prefactor value of $D_0 = 3 \times 10^{-15} m^2/s$ for C_6H_{14} in PS, which gives the best agreement with experimental data as shown later. Similarly, the diffusion coefficients of methanol in PMMA were found to be $3.7 \times 10^{-11} m^2/s$ at $38.5^{\circ}C$ and $4.5 \times 10^{-11} m^2/s$ at $40.5^{\circ}C$ (Ercken et al., 1996). Based on the Arrhenius relation, we estimate the prefactor D_0 to be $1.1 \times 10^{-10} m^2/s$ at $23^{\circ}C$ with $\phi = 0.25$. To match the experimental results, we make an adjustment that $D_0 = 3 \times 10^{-11} m^2/s$ for the PMMA-methanol system in the modeling.

3. Case II diffusion in a biaxially constrained thin film

3.1. The governing equations

In Section 2, we have formulated a nonequilibrium thermodynamic model to study non-Fickian diffusion of solvent in the glassy polymer. In this section and next one, we study case II diffusion process in a polymer thin film and a polymer sphere. When a glassy polymer thin film is submerged into a solvent-containing environment (Fig. 4a), the solvent molecules mainly diffuse along the thickness direction (x_3 in the Fig. 4a) in the film. For a laterally constrained thin film, we have

$$\lambda_1 = \lambda_2 = 1, \tag{33}$$

and

$$\sigma_3 = 0. \tag{34}$$

Using the Eqs. (33–34) and Eq. (15), we can obtain

$$\frac{\mu_B}{\lambda_3}\left(\lambda_3^2 - 1\right) + \frac{\mu_A}{\lambda_3}\left(\lambda_3^2 (\lambda_3^p)^{-2} - 1\right) + \frac{kT}{\Omega}\left[\ln\left(1 - \frac{1}{\lambda_3}\right) + \frac{1}{\lambda_3} + \frac{\chi}{\lambda_3^2}\right] - \frac{\mu - \mu_0}{\Omega} = 0. \tag{35}$$

The stresses of element "A" in Eq. (17) are written as

$$\sigma_3^A = \frac{\mu_A}{\lambda_3}\left(\lambda_3^2 (\lambda_3^p)^{-2} - 1\right) \tag{36}$$

$$\sigma_1^A = \sigma_2^A = \frac{\mu_A}{\lambda_3}\left((\lambda_1^p)^{-2} - 1\right). \tag{37}$$

The hydraulic pressure p^A, the equivalent shear stress τ^A, and the deviatoric stress s_i^A are given by Eqs. (24–26) respectively. We obtain the rates of plastic stretch $\dot{\lambda}_i^p$ from Eqs. (19–27) as

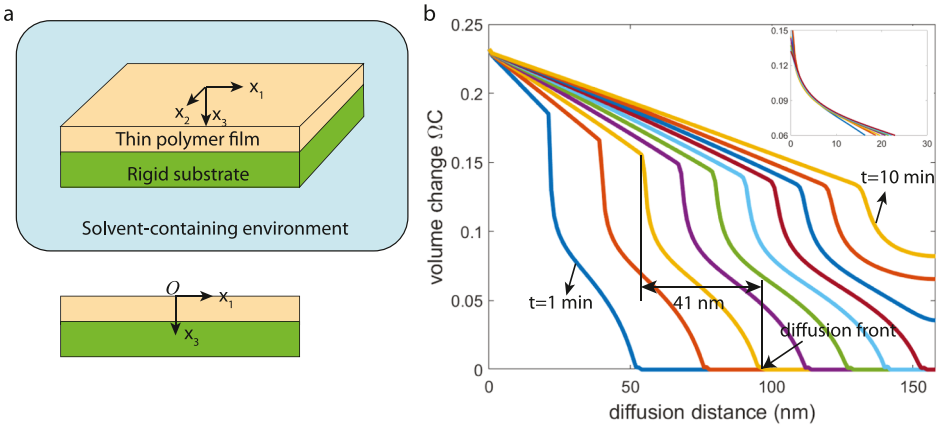

Fig. 4. (a) Schematic of case II diffusion in a glassy polymer film subject to biaxial constraint. (b) n-hexane penetrates into a PS film with a thickness of 158 nm. The inserted figure illustrates the overlaying of the profiles of solvent centration in the transition zone at different times. The volume change profile is captured every minute along thickness from 1 min to 10 min. The width of the transition zone is 41 nm which is comparable to the experiment result (Ogieglo et al., 2013).

$$\dot{\lambda}_i^p = \lambda_i^p \left[\dot{\gamma}_0 \left(\frac{\tau^A}{s_0} \right)^n \frac{s_i^A}{\tau^A} + \frac{p^A}{3\eta_0} \right] \exp(M\phi), \tag{38}$$

with $i = 1,2,3$. The linear kinetics law described by Eq. (31) is rewritten as

$$j_3 = -\left(\frac{CD}{kT} \right) \frac{\partial \mu}{\partial X_3} \tag{39}$$

with the volume change

$$\Omega C = \lambda_3 - 1. \tag{40}$$

Meanwhile, the mass conservation is given by:

$$\frac{\partial C(X_3,t)}{\partial t} + \frac{\partial j_3}{\partial X_3} = 0. \tag{41}$$

3.2. Results and discussions

We use the finite difference method to solve the series of partial differential equations derived above for the seven functions: $\mu(X_3, t)$, $C(X_3,t)$, $\lambda_3(X_3,t)$, $\lambda_1^p(X_3,t)$, $\lambda_3^p(X_3,t)$, $\dot{\lambda}_1^p(X_3,t)$, and $\dot{\lambda}_3^p(X_3,t)$. The boundary conditions entail that the stretch $\lambda_3(0,t) = \lambda_{eq}$, the chemical potential $\mu(0,t) = \mu_0$ and the solvent concentration $C(0,t) = C_0$, where $\Omega C_0 = \lambda_{eq} - 1$ with λ_{eq} being satisfied with

$$\frac{\mu_B}{\lambda_{eq}} \left(\lambda_{eq}^2 - 1 \right) + \frac{kT}{\Omega} \left[\ln\left(1 - \frac{1}{\lambda_{eq}} \right) + \frac{1}{\lambda_{eq}} + \frac{\chi}{\lambda_{eq}^2} \right] = 0, \tag{42}$$

based on Eq. (35).

The initial conditions specify the plastic stretches $\lambda_{10}^p = \lambda_{20}^p = \lambda_{30}^p = 1$, the chemical potential $\mu(X_3,0) = \mu_{dry}$, and solvent concentration $C(X_3,0) = 0$ (because the initial chemical potential of the solvent is very small).

The detailed computation steps are given as follows. First, for a given chemical potential profile $\mu(X_3,t)$, we compute the solvent

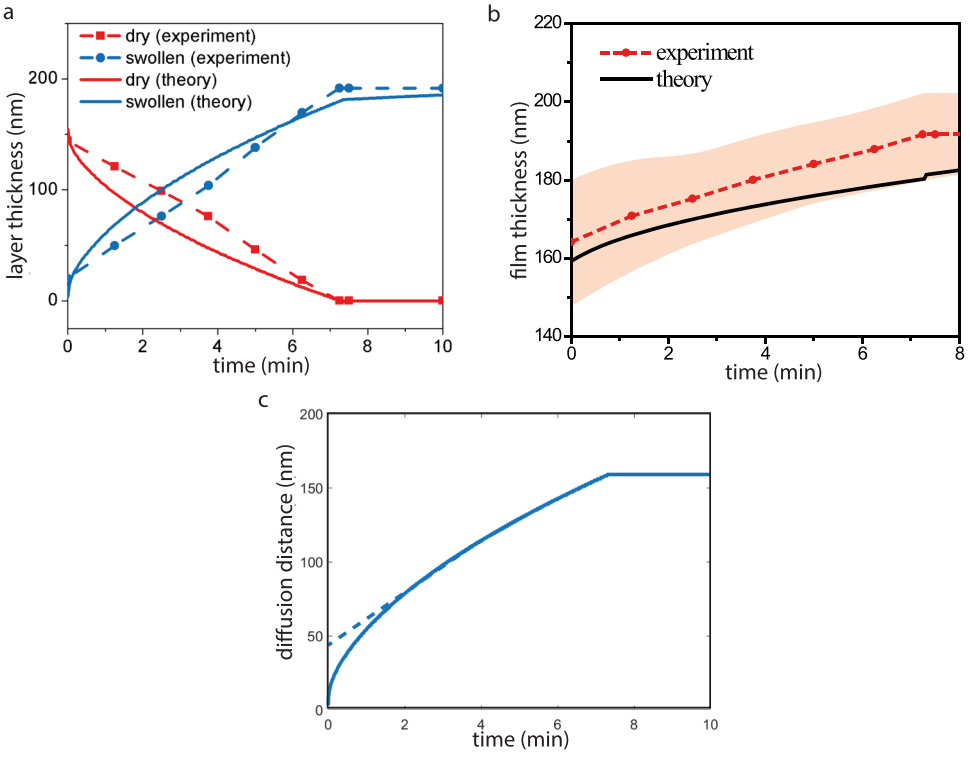

Fig. 5. (a) Thickness of the swollen and dry layers of a 158 nm PS film during the hexane sorption. (b) The total thickness of a 158 nm PS film during hexane sorption. The red dash line is the average value of experimental data, the red shadow is the range of experimental data, and the black solid line is the theoretical prediction. (c) The distance of diffusion front as a function of time. In (a) and (b), the solid lines are theoretical predictions; the dot-dash lines are experimental results from the reference (Ogieglo et al., 2013).

concentration $C(X_3,t)$ using Eq. (39) and Eq. (41), and then determine the stretch $\lambda_3(X_3,t)$ from the solvent concentration $C(X_3,t)$ using Eq. (40). With the value of $\lambda_3(X_3,t)$, we can calculate the plastic stretch rate $\dot{\lambda}_i^p(X_3,t)$ using Eq. (38) and Eqs. (24–26), and subsequently obtain the plastic stretch $\lambda_i^p(X_3,t)$ using

$$\lambda_i^p = \lambda_{i0}^p + \int_0^t \dot{\lambda}_i^p dt, \tag{43}$$

in which λ_{i0}^p is the initial plastic stretch along x_i. Finally, we update the chemical potential $\mu(X_3,t)$ for next time increment by employing Eq. (35). We repeat the above computation steps to obtain the full numerical solutions. In the numerical simulation of the solvent diffusion into PS, we use the parameters from Table 1. Herein, we simulate the solvent (i.e., n-hexane) penetrating into PS films with two different thicknesses (158 nm and 20 μm) which have been studied in the previous experiments (Ogieglo et al., 2013; P. Gall et al., 1990). And we compare our simulation results with the experimental measurements.

First, we study the evolution of the polymer swelling in a PS film with the thickness of 158 nm. Fig. 4b shows the solvent concentration (or the volume change) in the polymer film at different times. It is obvious that the solvent concentration profile in the polymer film is drastically different from what is expected from a Fickian diffusion system. In particular, a sharp transition zone connecting a dry polymer regime and nearly fully swollen regime exists in the film, which has also been frequently observed in the experiments of case II diffusion. Though the precise profile of the solvent concentration in the transition zone is very challenging to measure in the experiment, our model predicts that the transition zone width is around 40 nm, which is consistent with experimental results (Ogieglo et al., 2013). The tip of the transition zone is defined as the diffusion front as shown in Fig. 4b. Following the previous study (Hui et al., 1987b), we can define a steady state of case II diffusion in the glassy polymer when the penetrant's concentration profile of the transition zone is highly self-similar with respect to an observer moving with the front, as shown in the inserted figure of Fig. 4b. Based on our calculation, case II diffusion reaches a steady state when the diffusion time is between 0.3 min and 7.2 min for a

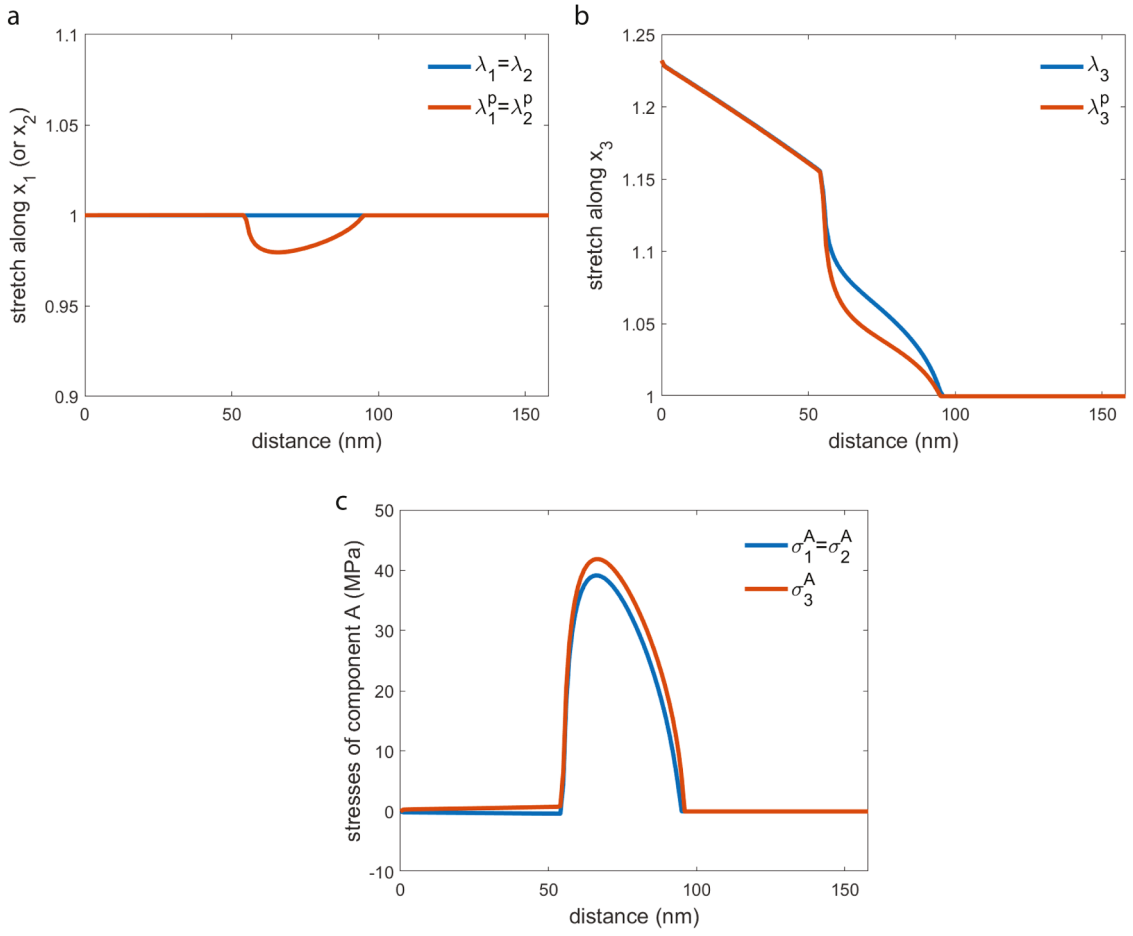

Fig. 6. The total stretches λ_1 (or λ_2) (a) and λ_3 (b), the plastic stretches λ^p_1 (or λ^p_2) (a) and λ^p_3 (b), and (c) the stresses in element "A": σ^A_1 (or σ^A_2) and σ^A_3, in PS film with a thickness of 158 nm at $t = 3$ *min*.

PS film with the thickness of 158 nm.

Moreover, we calculate the thicknesses of the dry region and the swollen region in the polymer film as a function of time as shown in Fig. 5a. The time required for the diffusion front to reach the constraint substrate across the 158 nm film is about 7.2 min, and this corresponds to an average moving velocity of the front of 1.32 $\mu m/hr$, which is consistent with the experimental measurement of 1.29 $\mu m/hr$ (Ogieglo et al., 2013). The quantitative difference between the theoretical predictions and the experiments is noticeable. There are several possible reasons for the discrepancy. The primary reasons for such difference include the simplifications of the current theoretical model and experimental inaccuracies. As a matter for fact, the experiment studies (Ogieglo et al., 2013) have provided the uncertainties of the thickness measurement of the PS film during hexane sorption. Fig. 5b plots the thickness of the entire PS film during hexane sorption and compares theoretical predictions and experiments. Our theorical predictions still fall within the range of experimental data. We plot the moving distance of the diffusion front in Fig. 5c, and our simulation shows that the velocity of the diffusion front in the steady state is nearly constant, which also agrees with the observation in the same experiment (Ogieglo et al., 2013). Fig. 5c also demonstrates that the velocity of diffusion front is faster initially, which has also been reported in case II diffusion in the glassy polymer (PMMA-methanol system) (Nixdorf et al., 2019).

Fig. 6 plots the total stretches (λ_1, λ_2 and λ_3), the plastic stretches (λ_1^p, λ_2^p and λ_3^p), and the stresses in element "A" at $t = 3$ min, corresponding to the orange curve in Fig. 4b. Due to the symmetry, the stretches and stresses along x_1 are the same as those along x_2. Within the sharp transition zone, the plastic stretch λ_3^p along x_3 is smaller than the total stretch λ_3, and λ_1^p is smaller than 1. As the plastic stretches (λ_1^p and λ_3^p) in the transition zone is smaller than the total stretch (λ_1 and λ_3), and according to Eqs. (36-37), the elastic stresses in element "A" along x_1 and x_3 directions are tensile in the transition zone, as shown in Fig. 6c. Based on Eq. (38), the elastic stresses in element "A" directly determine the rates of plastic stretch, which significantly impact the velocity of movement of the diffusion front.

We next analyze the penetration of n-hexane into PS film with a thickness of 20 μm. Fig. 7a plots the profile of the solvent concentration (or the volume change) in the film at different times. The solvent concentration profile in the thicker film is quite different from that in a thinner film shown in Fig. 4b. Our simulation shows that the solvent concentration profile in PS film of a 20 μm thickness changes with time, indicating that n-hexane diffusion in the PS film does not reach a steady state. This finding is different from the previous experiments done by P. Gall et al. (1990), where the PS-hexane system exhibited a self-similar sharp transition zone after the front advanced by approximately 1 μm, resulting in the transition zone width of about 1 μm in the steady state. However, an earlier work by Hui et al. (1987b) has also pointed out that the steady-state diffusion of hexane in the PS film is not possible if the film thickness is several micrometers. Moreover, in a recent study (Nixdorf et al., 2019), this extremely sharp transition zone in the steady state observed in the experiments by P. Gall et al. (1990) is speculated to be caused by the different diffusion rates of colorant used in the experiments to visualize the diffusion and n-hexane in the PS film. Though a direct observation of the transition zone in PS-hexane system has not been reported, in situ measurement of the transition zone has been conducted in PMMA-methanol system (Nixdorf et al., 2019). This study found that the width of the transition zone was about 90 μm, including a 30 μm sharply defined head and a 60 μm gentle tail. This width of transition zone obtained from the in situ measurement is much larger than the transition zone size obtained from the diffusion of the colorant (Thomas and Windle, 1978).

Fig. 7b plots the moving distance of diffusion front at different time in a 20 μm thick PS film. Even though the diffusion does not reach a steady state, the velocity of diffusion front is nearly constant after 200 h. Our study demonstrates the size effect on the solvent diffusion into glassy polymer. For n-hexane penetrating into a 20 μm PS film, our predicted velocity of the diffusion front is 0.024 $\mu m/hr$ (Fig. 7b), which is comparable with the measured velocity of the diffusion front about 0.036 $\mu m/hr$ (P. Gall et al., 1990). The velocity of diffusion front is much smaller than that in the thinner PS film as shown in Fig. 5.

The difference in the velocity of the diffusion front between a 158 nm PS film and a 20 μm PS film is related to the stress state in the transition zone. Fig. 8 plots the plastic stretches, the total stretches, and the stresses in element "A" of the 20 μm PS film at $t = 2 \times$

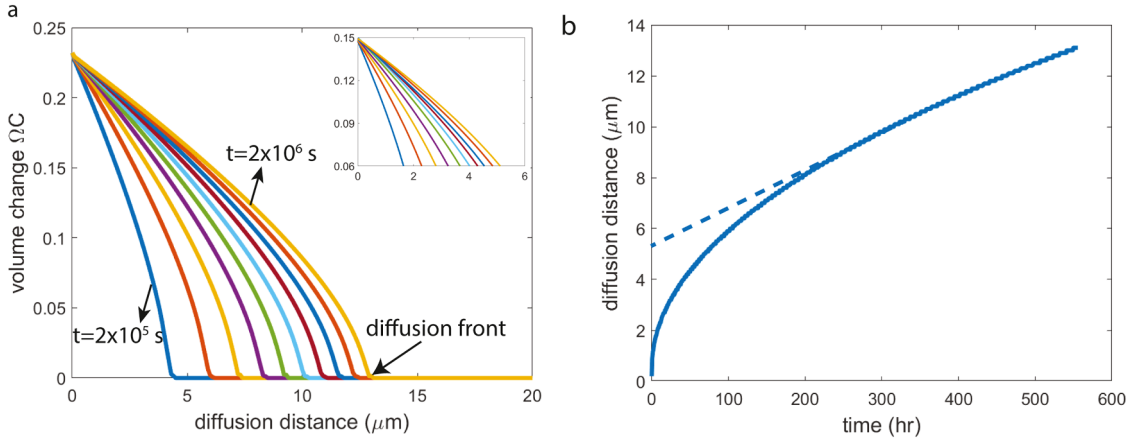

Fig. 7. n-hexane penetrates in PS film with a thickness of 20 μm. (a) The volume change profile is plotted for every 2×10^5 s along thickness. The inserted figure illustrates the overlaying of the profile of the concentration of solvent in the transition zone at different times. (b) The distance of diffusion front as a function of time.

$10^6 s$. Our results show that the difference between the plastic stretches and total stretches in the transition zone of the 20 μm PS film is significantly smaller than that of the 158 nm PS film. This small difference in stretches implies that the tensile stress of element "A" in the transition zone of the 20 μm PS film (Fig. 8c) is much smaller than that in the transition zone of the 158 nm PS film (Fig. 6c). Based on Eq. (38), the plastic stretch rate in the 158 nm PS film become much higher due to the larger tensile stress in element "A". As the velocity of the diffusion front in case II diffusion depends on the plastic flow rate, the velocity of diffusion front in the 158 nm PS film is much faster than that in the 20 μm PS film. Moreover, by comparing Fig. 4b and Fig. 7a, we can find that the size of the transition zone in the 158 nm PS film is much smaller than that in the 20 μm PS film.

4. Case II diffusion in a polymer sphere

4.1. Governing equations

For a spherical glassy polymer ball with a radius of A submerged in a solvent, the solvent migrates into the sphere along radial direction and a core–shell structure can form as sketched in Fig. 9a. The inner surface of the soft swollen shell is bonded with the dry and stiff core. With the increase of time, the shell thickens and the rigid core shrinks. The rigid core constraint causes an inhomogeneous stress and deformation field in the sphere. Force balance in the system requires that

$$\frac{d\sigma_r}{dr} + 2\frac{\sigma_r - \sigma_\theta}{r} = 0, \tag{44}$$

where the radial and hoop stresses from Eq. (15) are written as

$$\sigma_r = \frac{\mu_B}{\lambda_r \lambda_\theta^2}\left(\lambda_r^2 - 1\right) + \frac{\mu_A}{\lambda_r \lambda_\theta^2}\left(\lambda_r^2 \left(\lambda_r^p\right)^{-2} - 1\right) + \frac{kT}{\Omega}\left[\ln\left(1 - \frac{1}{\lambda_r \lambda_\theta^2}\right) + \frac{1}{\lambda_r \lambda_\theta^2} + \frac{\chi}{\left(\lambda_r \lambda_\theta^2\right)^2}\right] - \frac{\mu - \mu_0}{\Omega}, \tag{45}$$

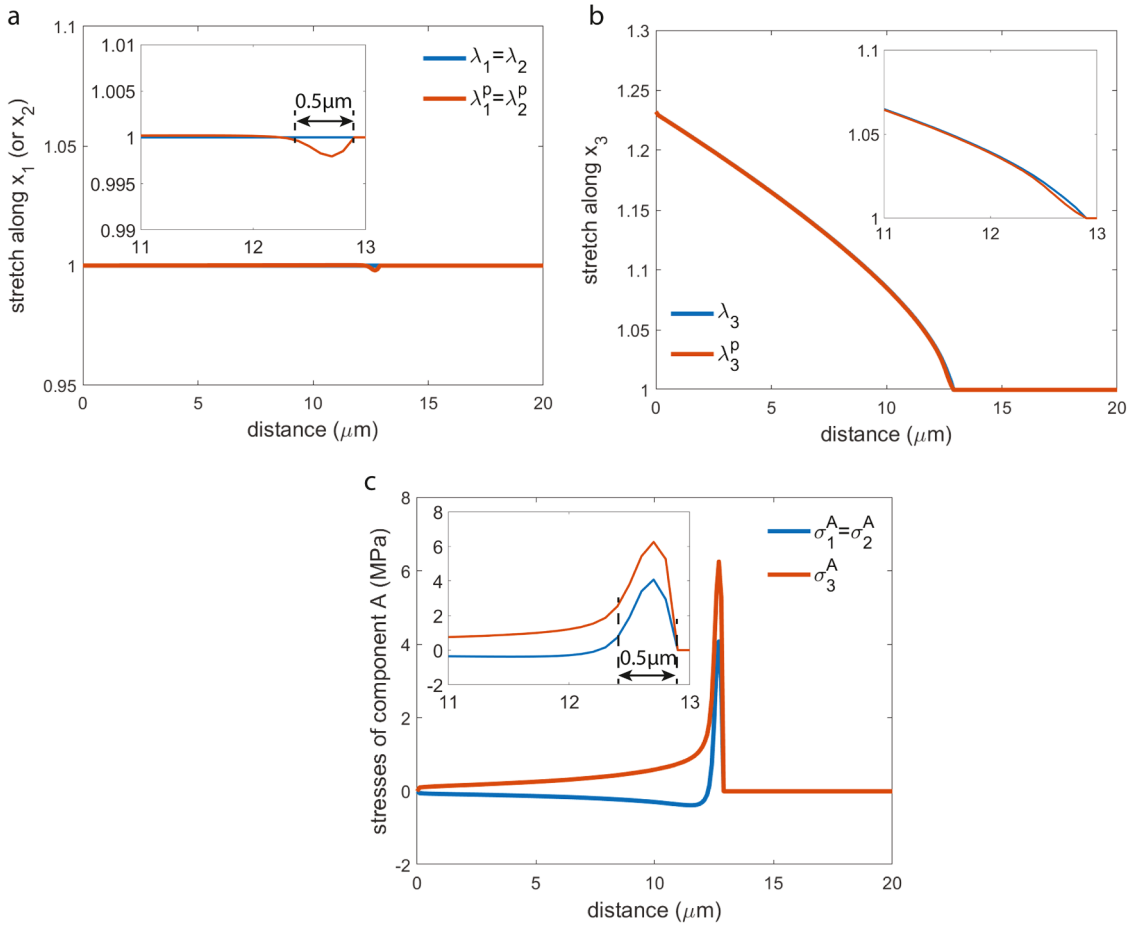

Fig. 8. The total stretches λ_1 (or λ_2) and λ_3, the plastic stretches λ_1^p (or λ_2^p) and λ_3^p, and the stresses in element "A" σ_1^A (or σ_2^A) and σ_3^A along thickness (x_3 direction), in PS film with a thickness of 20 μm at $t = 2 \times 10^6$ s.

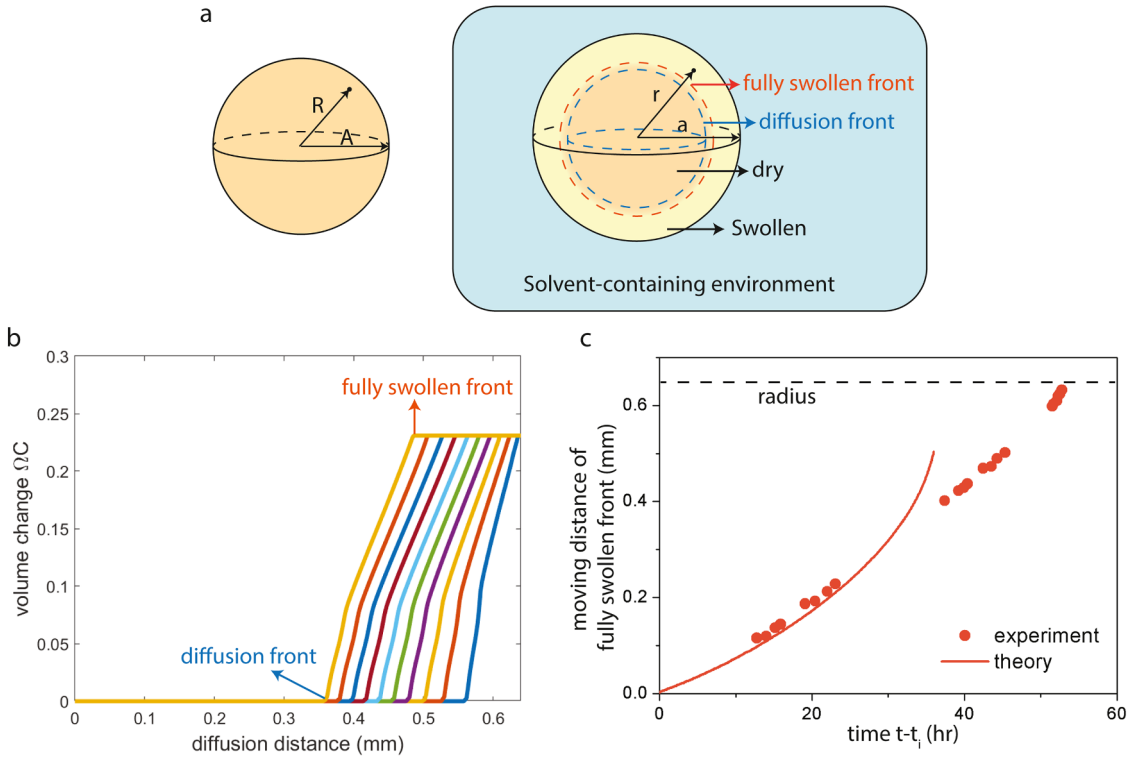

Fig. 9. (a) Schematic of free swelling of a polymer sphere (PMMA-methanol system). (b) The volume-change profile of a core-shell structure with a radius A of 0.64 mm is plotted for every $5 \times 10^3 s$. (c) The moving distance of the fully swollen front as a function of time, as the radius of the polymer sphere A in the reference state is 0.64 mm. t_i is the induction time which is the time required to reach the fully swollen state on the spherical edge. The solid line is the theoretical prediction; the solid dots are the experimental results from the reference (Li and Lee, 2006).

$$\sigma_\theta = \frac{\mu_B}{\lambda_r\lambda_\theta^2}\left(\lambda_\theta^2 - 1\right) + \frac{\mu_A}{\lambda_r\lambda_\theta^2}\left(\lambda_\theta^2(\lambda_\theta^p)^{-2} - 1\right) + \frac{kT}{\Omega}\left[\ln\left(1 - \frac{1}{\lambda_r\lambda_\theta^2}\right) + \frac{1}{\lambda_r\lambda_\theta^2} + \frac{\chi}{\left(\lambda_r\lambda_\theta^2\right)^2}\right] - \frac{\mu - \mu_0}{\Omega}, \tag{46}$$

with the radial stretch $\lambda_r = \frac{dr}{dR}$ and the hoop stretches $\lambda_\theta = \lambda_\phi = \frac{r}{R}$ in which R and r are the distances away from the center of core in the reference state and the deformed state respectively in Fig. 9a.

The surface of the sphere is stress-free, so

$$\sigma_r(r = a) = 0. \tag{47}$$

The stresses in the glassy polymer for element "A" in Eq. (17) are written as

$$\sigma_r^A = \frac{\mu_A}{\lambda_r\lambda_\theta^2}\left(\lambda_r^2(\lambda_r^p)^{-2} - 1\right), \tag{48}$$

$$\sigma_\theta^A = \sigma_\phi^A = \frac{\mu_A}{\lambda_r\lambda_\theta^2}\left(\lambda_\theta^2(\lambda_\theta^p)^{-2} - 1\right). \tag{49}$$

The corresponding hydrostatic pressure is

$$p^A = \frac{1}{3}\left(\sigma_r^A + \sigma_\theta^A + \sigma_\phi^A\right). \tag{50}$$

The deviatoric stress and effective shear stress have the same definition as Eqs. (25–26). The plastic stretch rates are

$$\dot{\lambda}_r^p = \lambda_r^p\left[\dot{\gamma}_0\left(\frac{\tau^A}{\tau_0}\right)^n \frac{s_r^A}{\tau^A} + \frac{p^A}{3\eta_0}\right]\exp(M\phi), \tag{51}$$

$$\dot{\lambda}_\theta^p = \dot{\lambda}_\phi^p = \lambda_\theta^p\left[\dot{\gamma}_0\left(\frac{\tau^A}{\tau_0}\right)^n \frac{s_\theta^A}{\tau^A} + \frac{p^A}{3\eta_0}\right]\exp(M\phi). \tag{52}$$

The kinetics law in a spherical coordinate system is

$$j_r = -\left(\frac{CD}{kT}\right)\frac{\partial \mu}{\partial R}. \tag{53}$$

The volume change of the polymer is

$$\Omega C = \lambda_r \lambda_\theta^2 - 1. \tag{54}$$

The mass conservation is written as

$$\frac{\partial C(R,t)}{\partial t} + \frac{\partial j_r}{\partial R} = 0. \tag{55}$$

4.2. Results and discussions

We next use finite difference method to solve the system of partial differential Eqs. (44–55) for the eight functions: $\mu(R,t)$, $C(R,t)$, $\lambda_r(R,t)$, $\lambda_\theta(R,t)$, $\lambda_r^p(R,t)$, $\lambda_\theta^p(R,t)$, $\dot{\lambda}_r^p(R,t)$, and $\dot{\lambda}_\theta^p(R,t)$. In the numerical computation, the boundary conditions entail that the radial stress $\sigma_r(A,t) = 0$, and the chemical potential $\mu(A,t) = \mu_0$. Meanwhile, the initial conditions specify the stretches $\lambda_r(R,0) = 1$ and $\lambda_\theta(R,0) = 1$, the plastic stretches $\lambda_{r0}^p = \lambda_{\theta 0}^p = 1$, the radial stress $\sigma_r(R,0) = 0$, the hoop stress $\sigma_\theta(R,0) = 0$, the chemical potential $\mu(R,0) = \mu_{dry}$ and the solvent concentration $C(R,0) = 0$.

The detailed simulation steps are described as follows. First, for a given chemical potential profile $\mu(R,t)$, we compute the solvent concentration $C(R,t)$ according to Eq. (53) and Eq. (55). Then we determine the stretch $\lambda_\theta(R,t)$ from the volume expansion that is the integration of ΩC from the spherical center to radius R, and calculate the stretch $\lambda_r(R,t)$ from the solvent concentration $C(R,t)$ using Eq. (54). With the values of $\lambda_r(R,t)$ and $\lambda_\theta(R,t)$, we can calculate the plastic stretch rates $\dot{\lambda}_r^p(R,t)$ and $\dot{\lambda}_\theta^p(R,t)$ with Eqs. (48–52) and Eqs. (25–26), and subsequently obtain the plastic stretch $\lambda_r^p(R,t)$ and $\lambda_\theta^p(R,t)$ by using the same equation shown in Eq. (43). In the reference

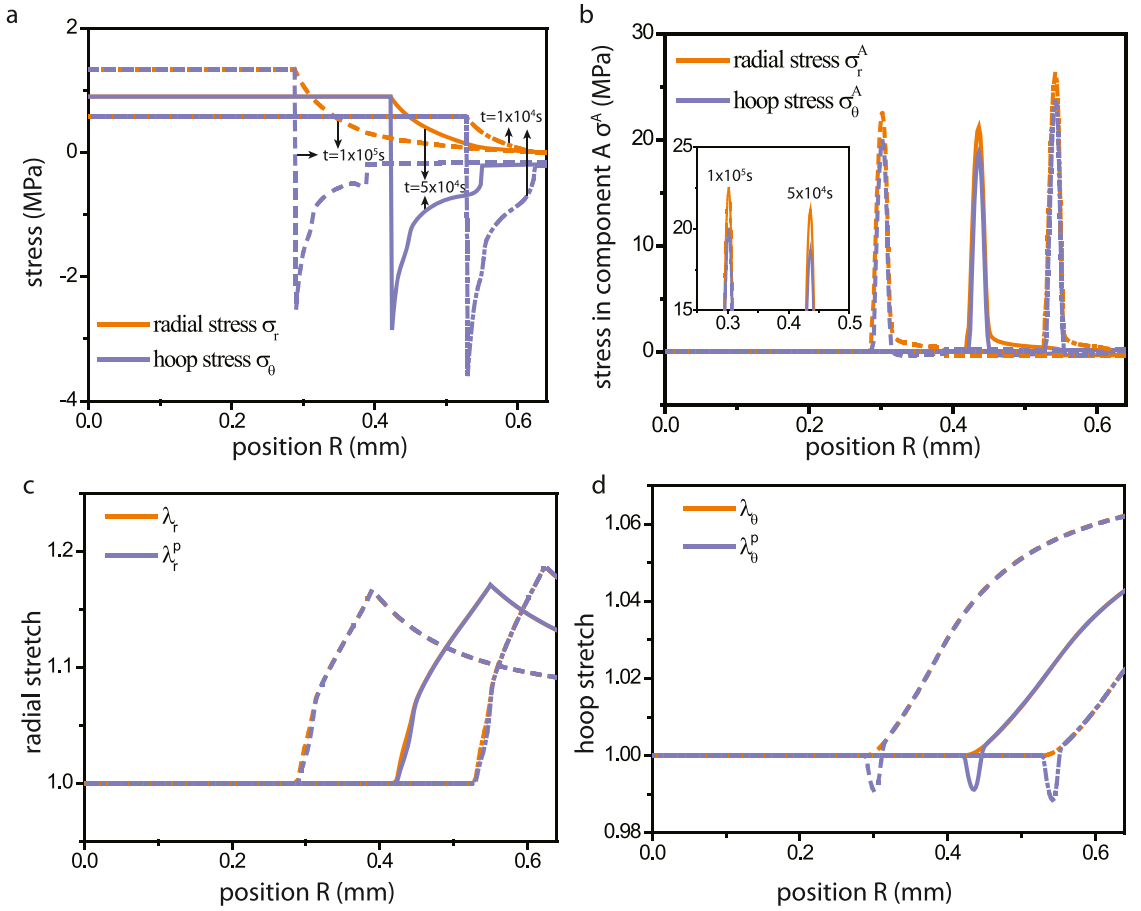

Fig. 10. The stress and stretch distribution in the core-shell structure when $t = 1 \times 10^4$ s (dash-dot lines), $t = 5 \times 10^4$ s (solid lines) and $t = 1 \times 10^5$ s (dash lines): (a) radial and hoop stresses (σ_r and σ_θ), (b) radial and hoop stresses in element "A" (σ_r^A and σ_θ^A), (c) radial stretches (λ_r and λ_r^p), and (d) hoop stretches (λ_θ and λ_θ^p).

state, Eq. (44) can be also rewritten as

$$\frac{d\sigma_r}{dR} = \frac{2(\sigma_\theta - \sigma_r)}{R}\frac{\lambda_r}{\lambda_\theta}. \tag{56}$$

Thereafter, we obtain the radial stress by integrating Eq. (56). Meanwhile, we calculate the hoop stress by using Eq. (46). Finally, we update the chemical potential $\mu(X_3, t)$ by employing Eq. (45) for the next time increment. We repeat above computation steps to obtain all these eight functions. In the numerical simulation of solvent diffusion into the glassy polymer sphere, we use the parameters from Table 1 (PMMA-methanol system) if not otherwise specified.

Fig. 9b plots the solvent concentration (or the volume change) in the polymer sphere with a radius of 0.64 mm along the radius at different times, and we use all the parameters from Table 1 to best fit the experimental results from reference (Li and Lee, 2006). The steady state of diffusion in the core-shell structure is achieved when the penetrant's concentration profile in the transition zone becomes self-similar. In the steady state, we can define diffusion front and fully swollen front and the width of the transition zone which is the distance between diffusion front and fully swollen front as shown in Fig. 9b. The width of the transition zone is 126 μm, which is comparable with the experimental value of around 90 μm (Nixdorf et al., 2019). Fig. 9c shows the moving distance of fully swollen front versus time $(t - t_i)$, where the induction time t_i is defined as the time required to reach the fully swollen state on the spherical edge. In a spherical core-shell structure, the moving velocity of the fully swollen front has two stages depending on its distance from the center. After the spherical edge is fully swollen, the moving velocity of the fully swollen front is almost a constant as long as the moving distance of the fully swollen front is less than 50% of the radius. Beyond this point, the diffusion velocity increases. These results are consistent with the experimental observations (Li and Lee, 2006).

Knowing the stress distribution in the core-shell structure is important for understanding the diffusion process in the glassy polymer. Fig. 10a illustrates the radial and hoop stress distribution in the core-shell structure at $t = 1 \times 10^4$ s, $t = 5 \times 10^4$ s and $t = 1 \times 10^5$ s, corresponding to Fig. 9. As shown in Fig. 10a, the hoop stress and radial stress in the dry core remains constant and in a tensile state. In the swollen shell, the hoop stress is compressive, while the radial stress is tensile. Furthermore, the hoop stress is nearly constant in the fully swollen shell. In the swollen zone, the radial stress is tensile and gradually decreases to zero at the surface.

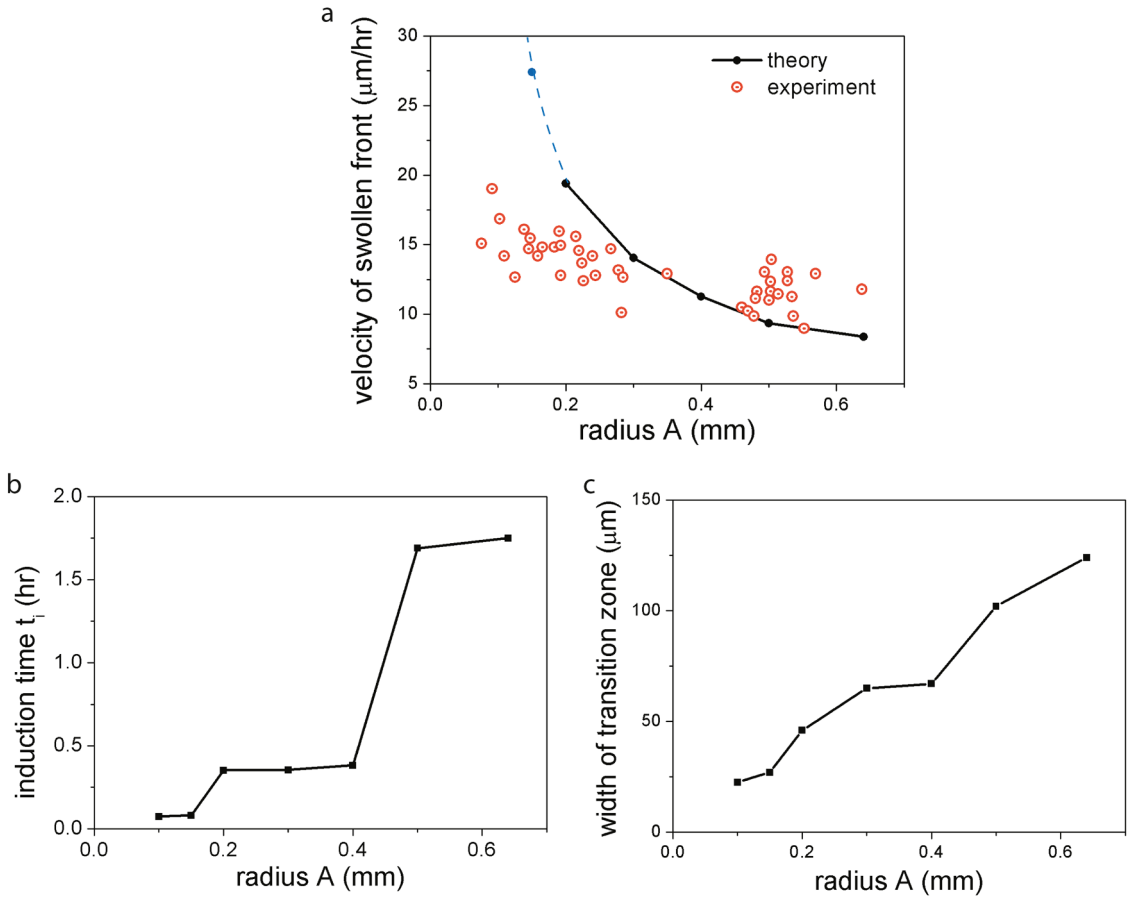

Fig. 11. (a) The diffusion speed, (b) the induction time t_i, and (c) the width of the transition zone as a function of radius R of the polymer sphere. In (a), the solid dot-line is theoretical prediction with using the parameters from Table 1; the open dots are experimental results from reference (Li and Lee, 2006).

Comparing the stresses in element "A" at $t = 5 \times 10^4$ s and $t = 1 \times 10^5$ s in Fig. 10b, the latter exhibits a little higher stress of element "A" in the transition zone. According to Eq. (51), this larger stress of element "A" leads to a higher plastic deformation rate, indicating a faster diffusion velocity, which is consistent with the result in Fig. 9c. The stress distributions associated with the stretches, which are shown in Fig. 10c–d.

Interestingly, case II diffusion in the core-shell spherical structure also exhibits size effects. We calculate the moving velocity of the swollen front in the core-shell spherical structure based on the time-dependent moving distance of the fully swollen front as shown in Fig. 9, considering only the moving distance of less than 50% of the radius. Fig. 11a plots the moving velocity of the swollen front as a function of the radius of the sphere using all the same parameters from Table 1. The velocity of the swollen front increases as the radius decreases. Our theoretical predictions agree well with the experimental data except for the case when the radius of the sphere is less than 0.15 mm, where the predicted swollen front velocity is larger than the experimental data. This velocity increase is related to the fact that the sphere radius is comparable with a critical length of the diffusion-relaxation relation, at which the diffusion time is comparable with the relaxation time of plastic flow.

In previous models, the induction time is assumed to be a material constant, which contradicts with experimental observations (Li and Lee, 2006). In our model, the induction time is also highly size-dependent as shown in Fig. 11b. Both our theory and Li's experiments indicate that the induction time approaches zero when the radius of the PMMA bead is less than 0.15 mm for the PMMA-methanol system. Moreover, our theory predicts that the width of the transition zone is also size-dependent, as shown in Fig. 11c. In summary, the diffusion velocity, the induction time and the width of the transition zone are all size dependent for case II diffusion in a polymer sphere.

5. Scaling behavior of case II diffusion in the glassy polymer

Vrentas et al. (1975) made a notable contribution to the study of polymer-solvent systems by introducing a dimensionless quantity, the diffusional Deborah number, which is defined as

$$De = \frac{\Lambda}{\Theta} = \frac{\text{characteristic relaxation time}}{\text{characteristic diffusion time}}. \tag{57}$$

The characteristic time for penetrant diffusion is written as $\Theta = \frac{L^2}{D}$ with L being a characteristic diffusion length and D being the diffusion coefficient of the penetrant in the polymer. Our model has two characteristic relaxation times of plastic flow of polymer chains: $\Lambda_{\text{vol}} = \frac{\eta_0}{\mu_A}\exp(-M\phi)$ for volumetric deformation and $\Lambda_{\text{shear}} = \frac{1}{\gamma_0}\exp(-M\phi)$ for shear deformation, which depend on the volume fraction of solvent in polymers. According to the data from Table 1, the characteristic relaxation time for shear deformation, Λ_{shear}, is significantly smaller than 1 s; and it can be ignored, as the timescales in experiments are much longer than 1 s. The time scale for the volumetric plastic deformation is more relevant for case II diffusion. Thus, we can rewrite Eq. (58) and define a critical length as

$$L_c = \sqrt{\frac{D_0\phi^2\eta_0\exp(-M\phi)}{\mu_B}}. \tag{58}$$

Based on Eq. (58), we can obtain the maximum critical length as $L_c^{max} = \frac{2}{eM}\sqrt{\frac{D_0\eta_0}{\mu_B}}$, when $\phi = \frac{2}{M}$. The maximum value of the critical length only depends on material properties. When the sample size is comparable to the maximum critical length L_c^{max}, the characteristic diffusion time is comparable to the characteristic time of plastic flow. This results in a situation where the solvent in the transition zone does not have enough time to reach chemical equilibrium. Consequently, the stretch in the spring of element "A" cannot fully relax, as

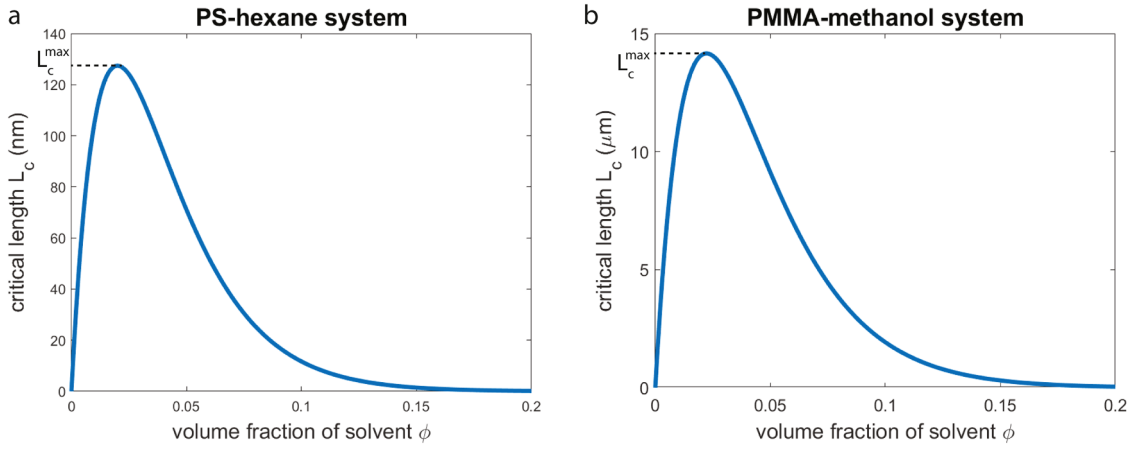

Fig. 12. The critical length for the case II diffusion of a solvent in a glass polymer as a function of the solvent concentration: (a) PS-hexane system and (b) PMMA-methanol system.

shown in Fig. 6, causing a tensile stress in the transition zone. However, as the sample size becomes much larger than the maximum critical length L_c^{max}, the elastic strain in the spring of element "A" in the transition zone can almost fully relax through the plastic flow of the dashpot of element "A", as shown in Fig. 8. This elastic-to-plastic transition in element "A" leads to a slower propagation of the diffusion front, which is consistent with the Argon's theory (Argon et al., 1999).

Considering the parameters in Table 1, we plot the length scale L_c as a function of the volume fraction of solvent in PS-hexane system and PMMA-methanol system as shown in Fig. 12. For PS-hexane system in Fig. 12a, the maximum critical length L_c^{max} is about 127 nm. Thus, the total stretch and plastic stretch in the diffusion front in the 158 nm PS film is very different as shown in Fig. 6. But the difference between the total stretch and plastic stretch in the 20 μm PS film is negligible as shown in Fig. 8. Fig. 12b shows that PMMA-methanol system has a maximum critical length L_c^{max} of 14.2 μm. The minimum radius of the polymer sphere we considered in Section 4 is 100 μm, which is seven times of maximum critical length L_c^{max}. We observe a dramatic increase in the propagation velocity of the diffusion front when $R \leq 150\ \mu m$ as shown in Fig. 11a.

6. Concluding remarks

In this article, we formulate a 3D model of case II diffusion in glassy polymers and compare our theoretical predictions with several different experimental studies. In the formulation, we integrate the elasto-visco-plastic constitutive model of the glassy polymer, the Flory-Rehner theory for polymer gels and the nonequilibrium thermodynamics. Our model predicts the stress field in the diffusion front which has been often ignored in previous studies. As the stress field is highly dependent on the sample size, the diffusion front velocity, the induction time and the width of diffusion front are all size-dependent. In particular, we predict that the moving velocity of the diffusion front dramatically increases when the sample size is comparable to the critical size given in Eq. (58). Our model also reveals that the propagation of the diffusion front accelerates as the diffusion distance is greater than 50% of the initial radius in the core-shell structure, which also agrees with the previous experimental observation. Even though we only studied the thin film and the core-shell structure as examples, the model proposed in this article can be used to study case II diffusion in glassy polymers with arbitrarily complex shapes. Admittedly, to make quantitative predictions for more general cases, complex numerical simulation code or integrating our model with finite element analysis tools, such as COMSOL MULTIPHYSICS, will be needed.

CRediT authorship contribution statement

Zhaoqiang Song: Methodology, Investigation, Project administration, Writing – original draft, Writing – review & editing. **Xu Li:** Investigation, Writing – review & editing. **Kaijin Wu:** Writing – review & editing. **Shengqiang Cai:** Conceptualization, Supervision, Investigation, Funding acquisition, Writing – review & editing.

Declaration of Competing Interest

The authors declare that there is no conflict of interest.

Data availability

All relevant data are within the paper.

Acknowledgments

SC acknowledges the support by the NSF through grant no. CMMI-2029145.

References

Argon, A.S., Cohen, R.E., Patel, A.C., 1999. A mechanistic model of case II diffusion of a diluent into a glassy polymer. Polymer (Guildf) 40, 6991–7012.
Baker, R.W., Lokhandwala, K., 2008. Natural gas processing with membranes: an overview. Ind. Eng. Chem. Res. 47, 2109–2121.
Baker, R.W., Low, B.T., 2014. Gas separation membrane materials: a perspective. Macromolecules 47, 6999–7013.
Bergstrom, J., 1998. Constitutive modeling of the large strain time-dependent behavior of elastomers. J. Mech. Phys. Solids 46, 931–954.
Bergström, J.S., Boyce, M.C., 2000. Large strain time-dependent behavior of filled elastomers. Mech. Mater. 32, 627–644.
Boyce, M.C., Kear, K., Socrate, S., Shaw, K., 2001. Deformation of thermoplastic vulcanizates. J. Mech. Phys. Solids 49, 1073–1098.
Boyce, M.C., Socrate, S., Llana, P.G., 2000. Constitutive model for the finite deformation stress–strain behavior of poly(ethylene terephthalate) above the glass transition. Polymer (Guildf) 41, 2183–2201.
Chang, Y.J., Chang, R.Y., Osswald, T.A., 2021. Measurement and modeling of bulk viscosity for polystyrene melts. Phys. Fluids 33 (7), 073103.
Chapuis, R.P., Aubertin, M., 2003. On the use of the Kozeny-Carman equation to predict the hydraulic conductivity of soils. Can. Geotech. J. 40, 616–628.
Colombo, P., Bettini, R., Santi, P., Peppas, N.A., 2000. Swellable matrices for controlled drug delivery: gel-layer behaviour, mechanisms and optimal performance. Pharm. Sci. Technol. Today 3, 198–204.
Ercken, M., Adriaensens, P., Reggers, G., Carleer, R., Vanderzande, D., Gelan, J., 1996. Use of magnetic resonance imaging to study transport of methanol in poly (methyl methacrylate) at variable temperature. Macromolecules 29, 5671–5677.
Flory, P.J., 1942. Thermodynamics of high polymer solutions. J. Chem. Phys. 10, 51–61.
Flory, P.J., 1953. Principles of Polymer Chemistry. Cornell university press.
Flory, P.J., Rehner, J., 1943. Statistical mechanics of cross-linked polymer networks I. Rubberlike elasticity. J. Chem. Phys. 11, 512–520.
Foreman, M.R., Vollmer, F., 2015. Optical tracking of anomalous diffusion kinetics in polymer microspheres. Phys. Rev. Lett. 114, 118001.

Gurtin, M.E., Fried, E., Anand, L., 2012. The Mechanics and Thermodynamics of Continua. Cambridge University Press, Cambridge.
Hajova, H., Chmelar, J., Nistor, A., Gregor, T., Kosek, J., 2013. Experimental study of sorption and diffusion of n-pentane in polystyrene. J. Chem. Eng. Data 58, 851–865.
Hong, W., Liu, Z., Suo, Z., 2009. Inhomogeneous swelling of a gel in equilibrium with a solvent and mechanical load. Int. J. Solids Struct. 46, 3282–3289.
Hui, C.Y., Wu, K.C., Lasky, R.C., Kramer, E.J., 1987a. Case-II diffusion in polymers. I. Transient swelling. J. Appl. Phys. 61, 5129–5136.
Hui, C.Y., Wu, K.C., Lasky, R.C., Kramer, E.J., 1987b. Case-II diffusion in polymers. II. Steady-state front motion. J. Appl. Phys. 61, 5137–5149.
Lee, E.H., 1969. Elastic-plastic deformation at finite strains. J. Appl. Mech. 36, 1–6.
Li, J.-X., Lee, P.I., 2006. Effect of sample size on Case II diffusion of methanol in poly(methyl methacrylate) beads. Polymer (Guildf) 47, 7726–7730.
Loeffel, K., Anand, L., 2011. A chemo-thermo-mechanically coupled theory for elastic–viscoplastic deformation, diffusion, and volumetric swelling due to a chemical reaction. Int. J. Plast. 27, 1409–1431.
More, A.P., Donald, A.M., Henderson, A., 1992. Stress modified Case II diffusion in poly(methyl methacrylate). Polymer (Guildf) 33, 3759–3761.
Mulliken, A.D., Boyce, M.C., 2006. Mechanics of the rate-dependent elastic–plastic deformation of glassy polymers from low to high strain rates. Int. J. Solids Struct. 43, 1331–1356.
Nealey, P.F., Cohen, R.E., Argon, A.S., 1995. Limited-supply non-Fickian diffusion in glassy polymers. Polymer (Guildf) 36, 3687–3695.
Nixdorf, J., Di Florio, G., Bröckers, L., Borbeck, C., Hermes, H.E., Egelhaaf, S.U., Gilch, P., 2019. Uptake of methanol by poly(methyl methacrylate): an old problem addressed by a novel raman technique. Macromolecules 52, 4997–5005.
Ogieglo, W., Wormeester, H., Wessling, M., Benes, N.E., 2013. Temperature-induced transition of the diffusion mechanism of n-hexane in ultra-thin polystyrene films, resolved by in-situ spectroscopic ellipsometry. Polymer (Guildf) 54, 341–348.
P Gall, T., Lasky, R.C., Kramer, E.J., 1990. Case II diffusion: effect of solvent molecule size. Polymer (Guildf) 31, 1491–1499.
Perry, K.L., McDonald, P.J., Clough, A.S., 1994. Case II diffusion in the PVC and acetone system. Magn. Reson. Imaging 12, 217–219.
Thomas, N., Windle, A.H., 1978. Transport of methanol in poly(methyl methacrylate). Polymer (Guildf) 19, 255–265.
Thomas, N.L., Windle, A.H., 1982. A theory of case II diffusion. Polymer (Guildf) 23, 529–542.
Vrentas, J.S., Jarzebski, C.M., Duda, J.L., 1975. A Deborah number for diffusion in polymer-solvent systems. AIChE J 21, 894–901.
Zhao, Z., Zhao, J., Hu, Z., Li, J., Li, J., Zhang, Y., Wang, C., Cui, G., 2019. Long-life and deeply rechargeable aqueous Zn anodes enabled by a multifunctional brightener-inspired interphase. Energy Environ. Sci. 12, 1938–1949.
Zhou, Q.Y., Argon, A.S., Cohen, R.E., 2001. Enhanced Case-II diffusion of diluents into glassy polymers undergoing plastic flow. Polymer (Guildf) 42, 613–621.
Zou, P., Nykypanchuk, D., Doerk, G., Xin, H.L., 2021. Hydrophobic molecule monolayer brush-tethered zinc anodes for aqueous zinc batteries. ACS Appl. Mater. Interfaces 13, 60092–60098.